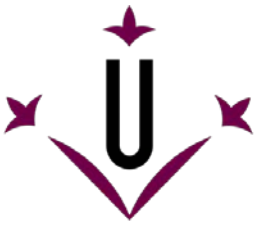

Extending the use of DGT to solutions where competition, saturation and kinetic effects are not negligible

Journal:	*Analytical Chemistry*
Manuscript ID	Draft
Manuscript Type:	Article
Date Submitted by the Author:	n/a
Complete List of Authors:	Jiménez-Piedrahita, Martín; Universitat de Lleida, Departament de Quimica Altier, Alexandra; Universitat de Lleida, Departament de Quimica Cecilia, Joan; Universitat de Lleida, Matemàtica Puy, Jaume; Universitat de Lleida, Departament de Quimica Galceran, Josep; Universitat de Lleida, Chemistry Rey-Castro, Carlos; Universitat de Lleida, Chemistry Zhang, Hao; Lancaster University, Lancaster Environment Centre Davison, William; Lancaster University, Environmental Science

Extending the use of DGT to solutions where competition, saturation and kinetic effects are not negligible

Martín Jiménez-Piedrahita[a], Alexandra Altier[a], Joan Cecilia[b], Jaume Puy[a], Josep Galceran[a], Carlos Rey-Castro[a], Hao Zhang[c] and William Davison[c]

[a]Departament de Química, [b]Departament de Matemàtica, Universitat de Lleida and AGROTECNIO, Rovira Roure 191, 25198, Lleida, Spain.

[c]*Lancaster Environment Centre, Lancaster University, Lancaster, United Kingdom*

* Phone number: 34 973 702529. Email: jpuy@quimica.udl.cat

Abstract

DGT (Diffusion Gradients in Thin films) was designed to sample trace metals in situ at their natural concentrations. The set-up and the experimental deployment conditions were established to allow interpretation of a linear accumulation of metal with time using a simple expression based on a steady-state flux under perfect sink conditions. However, the extension of DGT to a wide range of analytes and its use in varied conditions has shown that, in some situations, these conditions are not fulfilled, so that accumulations with time are non-linear. Previously, when such curvature was observed, concentrations in solution could not be reliably calculated. Here we present fundamentally derived equations which reproduce the time accumulation for three situations: i) kinetic limitations in the binding to the resin, ii) saturation or equilibrium effects or iii) non-negligible competitive effects. We show how the accumulations can be quantified in terms of the required kinetic and thermodynamic constants, and provide practical guidance for their use to obtain reliable estimates of solution concentrations. Solutions containing Mg or Mn, where all three situations can prevail, are used as examples. Calculated concentrations show reasonable agreement with the experimentally

known values and with the results of a numerical model of the system, significantly improving the estimations based on perfect sink conditions. Such an approach opens up the possibility of using DGT more widely in challenging systems and allows DGT data to be interpreted more fully.

Introduction

Diffusive Gradients in Thin films (DGT) was first developed for a time-averaged measurement of trace metals [1-5] and this is still the main application of the technique, although it has been extended to other analytes, such as oxyanions [6-8] and other inorganic and organic [9] components, as well as dissolved metal species released from nanoparticles [10-12]. Currently, there is an intensive research activity aimed at finding, testing and validating new binding layers to increase the range of target DGT analytes [6, 13-15]. Concomitantly, new applications have emerged. For instance, DGT has been rapidly established as a chemical imaging tool for solutes in sediments and soils [13]. Laser ablation ICP-MS of the DGT binding gel allows analyte fluxes and concentrations to be mapped at high spatial resolution. When the DGT device contains more than one type of binding layer or is coupled to planar luminescent sensors, simultaneous information on solute distribution and dynamics of several analytes can be obtained. This unprecedented information has furthered understanding of biogeochemical processes [16-19].

For many of these applications, DGT measurements are interpreted assuming perfect sink and steady-state conditions. However, there have been several reports that indicate that, even in aquatic systems, these conditions do not always apply. The possibility of competition from other ions in solution was recognised early in the development of DGT [20] and practical examples have emerged, including bicarbonate competing with the measurement of

phosphate using a ferrihydrite binding layer [21]. Some competition effects are observed as the effective capacity of the binding layer is approached, as for Fe competing with the measurement of Mn [22] and Ca competing with the measurement of Sr [23]. For ions at high concentrations, such as the major cations Ca and Mg, the straightforward capacity issue becomes a problem [24] especially when the ionic strength reduces noticeably the affinity of the binding to the Chelex. There have been examples of linear accumulations with time, but with less than theoretical slopes [25] and of the accumulation rate declining with time [26-28]. Although observations have sometimes been rationalised in general terms and there has been some attempt to quantify specific examples [20], there has been no systematic, quantitative treatment of how they arise. It is the aim of the present paper to examine quantitatively the consequences of non-ideal conditions in aquatic systems. We discuss the patterns of DGT accumulations that can arise, provide a check of the accuracy of the simple DGT expression and suggest new simplified, approximate expressions to determine the solution concentration when the simple expression is unsuitable. We focus on systems where the determinand does not react with other dissolved species (e.g. a metal in a solution without ligand). Section 2 is devoted to discussing the different regimes during the time evolution of the accumulation. Particular attention is paid to systems where perfect sink conditions are not reached and the accumulation is subject to kinetic limitations. Section 3 considers non-linear accumulations when the approach to equilibrium between the free and resin-bound metal cannot be neglected (i. e. due to capacity or saturation effects). Accumulation of Mg illustrates this behaviour. Section 4 deals with non-linear accumulations due to competition effects, as exemplified by the mixed system Mn/Mg. A numerical simulation code (see Supporting Information of [29]) to illustrate the processes that take place in the DGT device is used. This code is also used to check the accuracy of the analytical approximate expressions reported and the agreement of all these results with the experimental ones.

1. Regimes in the evolving metal accumulation

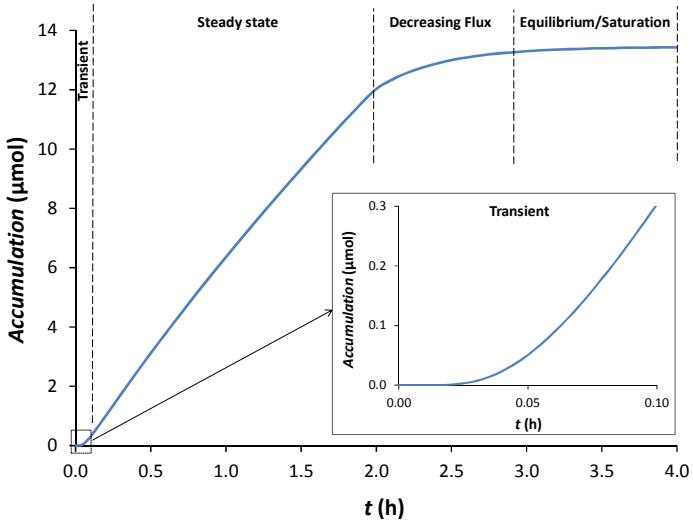

Figure 1. Metal accumulation as a function of time in a DGT device. Different regimes, separated by vertical dashed lines at somewhat arbitrary positions, can be recognized as indicated in the figure. Parameters of the simulation: $k_{a,R}$ *=1* $m^3 mol^{-1} s^{-1}$, $k_{d,R}$ $=10^{-3}$ s^{-1}, D_M $=4.94\times10^{-10}$ $m^2 s^{-1}$, δ^r $=4\times10^{-4}$ *m,* δ^g $=1.1\times10^{-3}$ *m,* $c_{T,R}$ *=28mol* m^{-3}, c_M^* *=10 mol* m^{-3}. *Insert: detail at short deployment times.*

Four different regimes [30-32] can be recognized in the time-series accumulation (plots of measured or simulated mass versus time, as in Fig.1.):

1.1 Transient regime

At short times, there is a transient regime (see inset in Fig.1) where the flux, which is proportional to the slope of the accumulation curve, increases while the first metal ions reach the resin layer and react with the resin sites. The upward bending curve, as indicated in Fig. 1, is characteristic of these conditions, providing a diagnostic tool for recognizing this behaviour. For standard DGT devices, t_{ss} in waters is of the order of 10 min [30].

1.2 Steady-state regime

A second regime corresponds to a linear accumulation of the metal as time increases. In this case, the flux is constant, indicating that the system is in quasi steady-state conditions. Two cases can be recognized. The first one, usually called the perfect sink regime, is fulfilled by most of the metals when Chelex is used as a binding layer. In this case, the association rate constant between the metal ion and the resin is so high that the binding is limited by the metal transport to the resin. Accordingly, the metal concentration at the resin-diffusive gel interface during this steady state regime drops to close to zero, the penetration of free metal ions in the resin domain is negligible and the DGT standard expression holds [3, 4]:

$$n = \frac{D_{\mathrm{M}} c_{\mathrm{M}}^{*}}{\delta^{\mathrm{g}}} A t \qquad (1)$$

where D_{M} is the diffusion coefficient of the metal, *n* stands for the accumulated moles, c_{M}^{*} for the metal concentration in the bulk solution, *A* for the effective area of the DGT device, *t* for the deployment time and δ^{g} is the thickness of the diffusion domain (also labeled Δg or g in previous works, [33]. The applicability of this equation has been checked for a wide range of deployment times, conditions and metals [2] and the penetration has also been checked by using DGT devices with a stack of two resin discs [34].

However, a steady state can also be attained when the kinetics of the metal association to the resin limits the accumulation while still far from equilibrium. Let us label this steady-state regime as "kinetically limited".

Practical indications of this regime are a (constant) slope of the accumulation vs time plot that is smaller than the one corresponding to limiting diffusion conditions, together with a non-negligible penetration of the metal in the resin domain, which can be verified using a DGT with multiple resin discs.

For metals, this case is not very common because, as predicted by the Eigen mechanism [35], a metal with slow binding to the resin will also have a small stability constant, so that equilibrium effects, also labelled as capacity effects [33], appear at short times, steady state no longer applies and the accumulation bends downwards, as indicated in the next regime.

With standard assumptions (steady state, excess of resin sites, negligible dissociation of bound metal, common diffusion coefficient of metal in the diffusive gel, filter and diffusive boundary layer), an analytical approximation for the metal accumulation in the resin in the kinetically limited case without capacity limitation can be written [36] as:

$$n = \frac{D_{\mathrm{M}}\, c_{\mathrm{M}}^{*}}{\delta^{\mathrm{g}} + \lambda_{\mathrm{M}} \coth\left(\frac{\delta^{\mathrm{r}}}{\lambda_{\mathrm{M}}}\right)} At \qquad (2)$$

where δ^{r} stands for the thickness of the resin domain,

$$\lambda_{\mathrm{M}} = \sqrt{\frac{D_{\mathrm{M}}}{k'_{\mathrm{a,R}}}} \qquad (3)$$

and $k'_{\mathrm{a,R}}$ is the product of $k_{\mathrm{a,R}}$ (the association rate constant) times the concentration of free resin sites, c_{R}. The term $\lambda_{\mathrm{M}} \coth\left(\frac{\delta^{\mathrm{r}}}{\lambda_{\mathrm{M}}}\right)$ is a measure of the effective distance of penetration of M, corresponding to the distance necessary for the metal concentration to drop to zero in the resin domain by linear extrapolation of the metal profile at the resin/diffusive gel interface. Accordingly, Eqn. (2) resembles Eqn. (1) when the region of transport by diffusion δ^{g} is replaced with $\delta^{\mathrm{g}} + \lambda_{\mathrm{M}} \coth\left(\frac{\delta^{\mathrm{r}}}{\lambda_{\mathrm{M}}}\right)$ and the slope of the accumulation plot can be used to obtain $k_{\mathrm{a,R}}$, which can also be found from the percentage of mass accumulated in the back resin disc [32, 36].

Accumulation of Mg in DGT devices with a stack of two resin discs deployed in 100 mol m^{-3} $NaNO_3$ solution at pH 7.5 serves as an experimental example of accumulation under kinetic limiting conditions. Indeed, as can be seen in Fig. 2, the accumulation in a solution of 0.09 mol m^{-3} Mg is almost linear for times smaller than 10 h, with a slope smaller than that of the perfect sink case (dotted line). For longer deployment times, the accumulation bends downwards, indicating that equilibrium effects are non-negligible and steady-state conditions are lost.

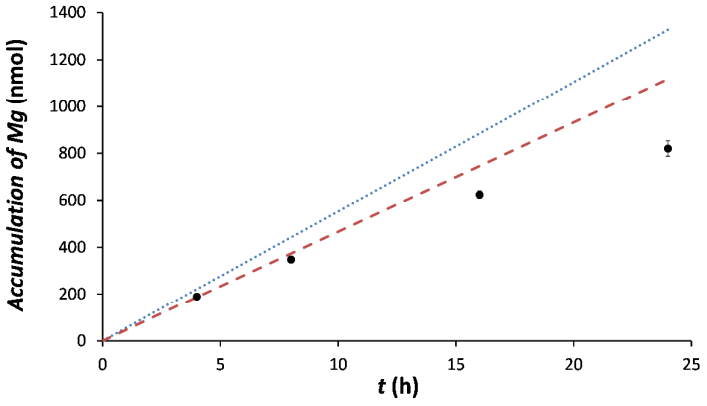

Figure 2. Time evolution of the total accumulation of Mg in DGT devices with two resin discs. Markers correspond to experimental accumulations at salt background concentrations of 100 mol·m^{-3} at pH 7.5. Dashed line corresponds to results obtained with Eqn.(2) when $k_{a,R}$ *=1.7×10^{-4} m^3 mol^{-1} s^{-1} and* $k_{d,R}$ *=10^{-4} s^{-1}. Dotted line corresponds to Mg accumulation obtained with Eqn. (1). Other parameters:* D_M *=4.94×10^{-10} m^2s^{-1},* δ^r *=8×10^{-4} m,* δ^g *=1.1×10^{-3} m,* $c_{T,R}$ *=28mol m^{-3} and* c_M^* *=0.09 mol m^{-3}.*

The use of Eqn. (2) to calculate $k_{a,R}$ requires the determination of the slope at short times before downward bending starts. Using the first data point, we obtained $k_{a,R}$ =1.7×10^{-4} m^3 $mol^{-1}s^{-1}$, which introduced in Eqn. (2) yields the dashed line in Fig. 2.

1.3 Decreasing flux regime

At longer times, the accumulation bends downwards, indicating that it approaches the equilibrium value and the flux decreases as time increases. The accumulation is lower than expected from perfect sink conditions and one can say that the accumulation is thermodynamically limited. Manifestation of these effects on DGT measurements has been reported in previous development studies [6, 15, 21, 27], and this regime, which will be discussed in the next Section, has also been termed "saturable" [37] or “mixed” [31]. A special case of the decreasing flux regime arises for deployments in soils and sediments. Due to the extension of the diffusion profile into the soil or sediment domain, the steady state regime cannot be reached and instead, a decreasing flux regime is registered.

1.4 Equilibrium/saturation regime

Finally, at sufficiently long times, the accumulation reaches a plateau, indicating negligible net metal binding (Fig. 1). Accordingly, there are no metal concentration gradients, *i.e.*: the free metal concentrations in the resin domain and bulk solution are in equilibrium (both concentrations are equal or related by a Boltzmann factor when the charge of the resin sites is not sufficiently screened by the background salt) and the bound metal is in equilibrium with the free metal concentration. We will refer to this situation as the equilibrium situation, but it could also be referred to as the situation where the “effective capacity” of the DGT device has been reached as done in [38]. The amount accumulated when equilibrium is achieved (equilibrium accumulation or the “effective capacity”) increases as metal concentration increases until it reaches a maximum that we associate with saturation: all the resin sites (the total capacity) are occupied.

2. Saturation and equilibrium effects

Now, we consider in more detail the situations described in Sections 1.3 and 1.4, where steady state no longer applies and the accumulation curve bends downwards as seen in Fig. 1.

Assuming that all the resin sites show a fixed affinity for the metal, the net binding rate can be written as

$$\frac{\partial c_{\mathrm{MR}}}{\partial t} = k_{\mathrm{a,R}} c_{\mathrm{M}} c_{\mathrm{R}} - k_{\mathrm{d,R}} c_{\mathrm{MR}} \quad (4)$$

where c_{M} and c_{R} are the local concentrations of free M and free resin sites at the spatial position considered and $k_{\mathrm{d,R}}$ is the kinetic dissociation rate constant. The first term on the right hand side of Eqn. (4) (4)stands for the association rate, while the second one quantifies the dissociation.

A decrease of the net binding arises from both the increase of the rate of dissociation (due to the increase of c_{MR}) and the decrease of the association rate (due to the decrease of c_{R}) as Eqn. (4) indicates. Dissociation is non-negligible when equilibrium (or "effective capacity") between bound and bulk free metal is approached. The decrease of the association term is non-negligible when equilibrium is closely approached or when competitive effects are relevant as will be discussed in the next Section.

Fig. 3 shows a clear case where thermodynamic limitations due to equilibrium have been observed. It corresponds to Mg binding to DGT devices with a stack of two resin discs that were deployed in a 500 mol m^{-3} $NaNO_3$ solution at pH 7.5. (Details of the experimental setup can be found in [39]).

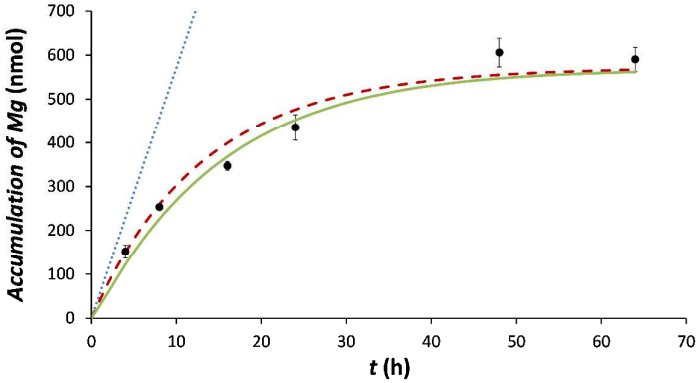

Figure 3. Evolution of Mg accumulation at salt background concentration ($NaNO_3$)= 500 mol m^{-3}. Markers: experimental accumulations (both discs) in DGT devices with a stack of two resin discs at pH=7.5. Continuous line stands for numerical simulation, dashed lines for results obtained with Eqn. (5) and dotted line for results obtained with Eqn. (1), i.e. corresponding to perfect sink conditions. $k_{a,R}$ *=7.0×10^{-5} m^3 mol^{-1} s^{-1},* K_{MR} *=0.7 m^3 mol^{-1},* Π_{Mg} *=1.1,* c_M^* *=0.093 mol m^{-3}. Other parameters as in Fig. (2).*

The reduction in the rate of metal accumulation (see markers in Fig. 3) is so noticeable with respect to the perfect sink accumulation (dotted line in Fig. 3) that a quasi-flat trend appears at long times, indicating that equilibrium conditions have been reached. Fig. 3 also shows, in continuous line, the accumulation calculated with numerical simulation after fitting the equilibrium and kinetic association constants to the experimentally obtained total accumulation and to the percentage in the back binding layer [39]. With these parameters, the simulation tool has also been used to plot the concentration profiles corresponding to different times (Fig. 4).

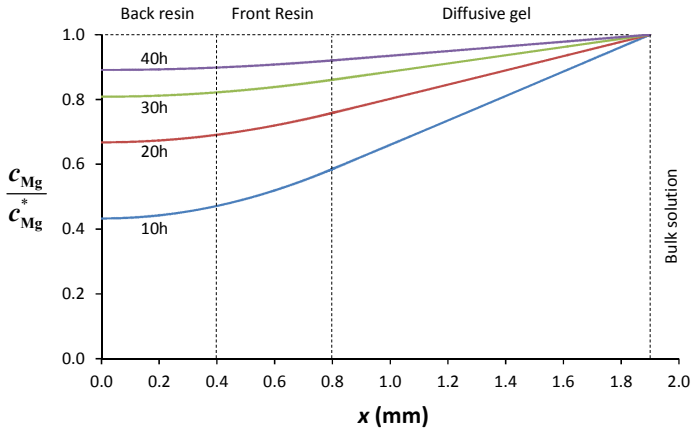

Figure 4. Normalized Mg concentration profiles at time 10, 20, 30 and 40 h for the conditions of Fig. 3. Vertical dashed lines indicate the frontiers of each resin gel disc.

The approach to equilibrium is confirmed by the increase of the average free metal concentration in the resin domain as time increases as seen in Fig. 4. When the concentration of unbound metal in the resin approaches the bulk solution concentration, at *t*>40h (See Fig. 4), there is almost no net accumulation (the rate of association is close to that of dissociation) as seen at the rightmost part of Fig. 3.

In attempting to quantify the approach to equilibrium between the bound and free metal, one can assume, as an approximation, that the concentration profile of the free metal is homogeneous in the resin domain and linear in the diffusive disc (as Fig. 4 approximately shows). As demonstrated in the SI, the accumulation for $K_{MR}c_{TR} \ll 1$ can be approximated as:

$$n_T(t) = A\delta^r c^r_{MR}(t) = \frac{A\delta^r c_{TR}\Pi K_{MR} c^*_M\left(1-e^{-bt}\right)}{1+\Pi K_{MR} c^*_M\left(1-e^{-bt}\right)} \quad (5)$$

where

$$b = \left(k_{d,R} - F - H\right)/2 \quad (6)$$

$$F = -\left(\frac{D_M}{\Pi\delta^r\delta^g} + k'_{a,R}\right) \quad (7)$$

$$H = \sqrt{F^2 + 2Fk_{d,R} + 4k'_{a,R}k_{d,R} + k^2_{d,R}} \quad (8)$$

$c_{\mathrm{MR}}^{\mathrm{r}}(t)$ labels the homogeneous bound metal concentration in the resin domain, as assumed in this approximation, and Π is the Boltzmann factor corresponding to the partitioning of the metal at the resin-diffusive gel interface due to any electrostatic effects of the resin charges not screened by the background salt.

At long times, the exponential terms disappear and Eqn. (5) tends to $n_{\mathrm{T}}(t \to \infty) = A\delta^{\mathrm{r}} c_{\mathrm{MR}}^{\mathrm{eq}}$, where $c_{\mathrm{MR}}^{\mathrm{eq}} = \frac{c_{\mathrm{TR}} \Pi K_{\mathrm{MR}} c_{\mathrm{M}}^{*}}{1 + \Pi K_{\mathrm{MR}} c_{\mathrm{M}}^{*}}$ is the concentration of bound metal in equilibrium with the free metal concentration in the resin domain (equal to Πc_{M}^{*}). The accuracy of Eqn. (5) can be assessed by comparing the accumulations calculated with Eqn. (5) and those obtained with rigorous numerical simulation with the same set of parameters. Some figures with this comparison are reported in Section 1 of the SI. The similar accumulations demonstrate good accuracy in the range of the stability constants studied.

Eqn. (5) applies to standard DGT devices. For a DGT with a stack of resin discs, one just needs to indicate the corresponding resin thickness (double thickness, $\delta^{\mathrm{r}} = 8 \times 10^{-4}\mathrm{m}$, for a stack of two resin discs). A good agreement between Eqn. (5), plotted with dashed line, with numerical simulation results and experimental accumulations can be seen in Fig. 3 using the Mg binding parameters estimated in [39] and reported in the caption of Fig. 3. Experimental values of the Boltzmann factor Π were obtained by adding a small amount of Rb in the system which allows measuring Π as the ratio of the Rb concentration in the resin domain with respect to the Rb bulk concentration in solution, as explained elsewhere [39]. If the Mg binding parameters, diffusion coefficients and the characteristic lengths of the DGT device are known, Eqn. (5) can be used to determine c_{Mg}^{*} from the experimental Mg-binding data depicted in Fig. 3. The bulk Mg concentration thus determined is reported in Table (1) which indicates a very good agreement with the true experimental value and a substantial improvement with respect

to the value determined by using Eqn. (1) which retrieved values with increasing errors for longer accumulation times. The practical application of Eqn. (5) to unknown samples requires, then, the knowledge of the binding parameters of Mg at the pH and ionic strength of the system. This information can be found in an appropriate database or can be obtained from a dedicated experiment measuring the Mg accumulation in a system of known Mg concentration under the experimental conditions of interest and then fitting the accumulation results to Eqn. (5).

Table 1. Estimation of c^*_M using the perfect sink approximation (Eqn. (1)) or using Eqn. (5), when they are applied to the Mg binding data at different deployment times using the parameters reported in Fig. 3.

I (M)	t(h)	c^*_{Mg} used in the simulation (mol m^{-3})	c^*_{Mg} calculated (mol m^{-3})	
			from Eqn. (5)	from Eqn. (1)
0.5	4	0.093	0.092	0.063
	8			0.052
	16			0.035
	24			0.030
	48			0.021
	64			0.015

3. Competition effects

Competition effects arise when the amount of one metal bound to the resin depends, for a fixed bulk metal concentration of the analyte, on the concentration of other cations present in the system [21, 25]. In ref. [25], Tankéré-Muller and co-workers reported the influence of Mg on the accumulation of Mn. This study is here extended by considering different Mg concentrations at ionic strength, 155 mol m^{-3}, and pH 5.5 as used in [25]. Fig. 5 reports the results, while the experimental details are given in Section 6 of the SI. According to previous

reporting [25], Mn accumulation follows the trend of perfect sink conditions when the ionic strength in the system is 10 mol m^{-3}. However, Mn accumulation at 24 h deployment is only half of the perfect sink expectation (dashed line in Fig. 5) when the ionic strength has increased from 10 to 155 mol m^{-3} by adding only NaCl into the system (compare dashed line with red square markers in Fig. 5). The decrease and the bending of the Mn accumulation reflects the decrease of the stability constant of the Mn binding to the Chelex due to the screening of the electric charge by the salt background. According to the Chelex 100 Instruction manual from Bio-Rad [40], the transition metal that binds most weakly is Mn, making it most prone to such an effect.

However, by keeping the ionic strength fixed, and replacing part of the NaCl by increasing concentrations of $MgCl_2$, further reductions of the Mn accumulation arise. These decreases evidence the competing effects between Mg and Mn and they can be understood recalling that the binding of Mg reduces c_R, and, thus, the Mn association rate (first term in Eqn. (4)) is reduced. Accordingly, both the slope of the Mn accumulation at short times and the plateau reached by the Mn accumulation decrease as the Mg concentration increases. Both effects are evident in Fig. 5.

A quantitative analysis was undertaken with the simulation tool used in section 3. Details of the mathematical formulation, boundary conditions and numerical resolution can be found in section 3 of the SI. The fitting of the simulations to the experimental values (markers in Fig. 5) provided the kinetic constants of the Mn and Mg binding. Details of this process, kinetic parameters and calculated accumulation plots are described in the SI, section 5.

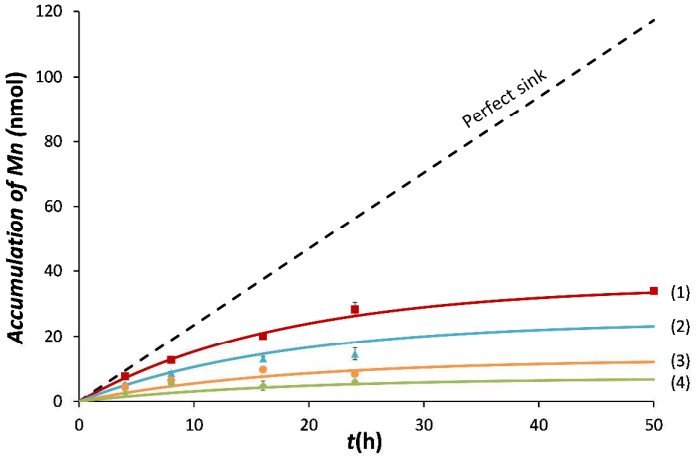

Figure 5. Mn accumulation in a standard DGT device from a solution with c^*_{Mn} *= 3.64×10^{-3} mol m^{-3} in the presence of different concentrations of Mg where the ionic strength was maintained at 155 mol m^{-3} using appropriate concentrations of NaCl for each solution: Dashed line corresponds to perfect sink approximation. Markers correspond to experimental values for: only Mn (squares),* c^*_{Mg} *=5.5 mol m^{-3} (triangles),* c^*_{Mg} *=27.7 mol m^{-3} (circles) and* c^*_{Mg} *=60.8 mol m^{-3} (diamonds). Continuous lines are calculated with Eqn. (9) for: only Mn (label 1),* c^*_{Mg} *=5.5 mol m^{-3} (label 2),* c^*_{Mg} *=27.7 mol m^{-3} (label 3) and* c^*_{Mg} *=60.8 mol m^{-3} (label 4). Other parameters used:* $k_{a,MnR}$ *=4.0×10^{-4} m^3 mol^{-1} s^{-1},* K_{MnR} *= 2.35 m^3 mol^{-1},* $k_{a,MgR}$ *=1.9×10^{-5} m^3 mol^{-1} s^{-1},* K_{MgR} *=0.13 m^3 mol^{-1},* D_{Mn} *=5.39×10^{-10} m^2 s^{-1} and* D_{Mg} *=4.94 ×10^{-10} m^2 s^{-1}.*

Alternatively, some approximate analytical solutions can be written based on Eqn. (5) once it is extended to consider competition effects. As derived in section 2 of the SI, the accumulation of Mn in the present conditions can be approximately described by

$$n_{T,Mn}(t) = A\delta^r \frac{c_{TR}}{1+\Pi K_{MgR} c^*_{Mg}} \Pi K_{MnR} c^*_{Mn} \left(1 - e^{-k_{d,Mn} t/2}\right) \quad (9)$$

The agreement of Eqn. (9) with the rigorous numerical simulation for a common set of parameters in the range of those reported for the Mn and Mg binding can be seen in Section 2.2 of the SI. The accuracy of Eqn. (9) is quite good when using the set of parameters obtained for Mn accumulations of Fig. 5 from the rigorous numerical simulation (see section 5 of the SI). This suggests that the kinetic parameters of the Mn binding and the stability constant of Mg

can also be determined with Eqn. (9), thus avoiding the use of the numerical simulation. In order to reduce the number of unknowns to be fitted simultaneously, the kinetic parameters of Mn can be determined from the Mn accumulation in absence of Mg, while the stability constant of Mg is then obtained from the accumulations with the presence of Mg in the system. The results are reported in Table (2), while Fig. 5 depicts in continuous line the corresponding calculated accumulations. The agreement with experimental data is quite reasonable and similar to that of the numerical simulation reported in the SI. It could, then, be concluded that for this system, the simple Eqn. (9) is able to give a good agreement with the experimental data with kinetic and thermodynamic values in the order of those obtained by using more sophisticated numerical methods.

Table 2. Kinetic parameters of Mn and stability constant of Mg derived using Eqn (9) to fit the accumulation data at ionic strength 155 mol m^{-3} and pH 5.5 reported in Fig. 5. Parameters used are those reported in the caption of Fig. 5.

	$k_{a,R}$ (m^3 mol^{-1} s^{-1})	$k_{d,R}$ (s^{-1})	K_{MR} (m^3 mol^{-1})
Mn	7.48×10^{-5}	3.1×10^{-5}	2.41
Mg	-	-	0.07

The reported values are conditioned to temperature, ionic strength and pH, which is why the value of K_{MgR} in Table (2) diverges from that in the caption of Fig. 3. Actually, pH has an important influence on the K_{MgR} as can be seen by comparing the value reported in Table (2) of [39] (ca. 1.7 m^3 mol^{-1} for I=100 mol m^{-3}, pH =7.5) with the value here reported in Fig. 5 (0.13 m^3 mol^{-1} for I=155 mol m^{-3}, pH =5.5). The decrease of one order of magnitude of K_{MgR} from pH 7.5 to pH 5.5 can also be considered a competing effect of H^+ on the Mg binding.

The main reduction of the accumulation of Mn is due to the I raising from 10 to 155 mol m^{-3}, which lowers the binding constant and so, the effective capacity of Chelex for Mn. Competition effects (Mg–Mn) additionally reduce the Mn accumulation.

The application of Eqn. (9) to determine c^*_{Mn} requires the knowledge of c^*_{Mg}, K_{MgR}, K_{MnR}, $k_{d,Mn}$, Π as well as the geometrical parameters of the DGT device. These parameters have to be determined in dedicated experiments at the pH, temperature and ionic strength of the sample. In the present case, it has been quite simple, since Mn and Mg parameters could be determined in separate experiments with only one metal in the system. Once these parameters are known, the concentration can be calculated from the accumulation. Applying this process to the accumulations shown in Fig 5, one obtains the c^*_{Mn}-values reported in Table (3), which indicates a reasonable agreement with the experimental values, significantly improving the estimations based on perfect sink conditions. The highest error arises for the highest Mg concentration since the accumulation is, then, the lowest thereby increasing the relative error of Eqn. (9).

Table 3. Calculation of c^*_{Mn} using the perfect sink approximation (Eqn. (1)) or the competition approximation, Eqn. (9), in the Mg/Mn competing system with parameters and Mn experimental accumulations reported in Fig. 5 at 24 h.

Experimental bulk concentrations (mol m^{-3})		c^*_{Mn} calculated (mol m^{-3})	
c^*_{Mn}	c^*_{Mg}	From Eqn. (1) (Perf. Sink)	From Eqn. (9) (competition explicitly included)
3.64×10^{-3}	5.3	9.02×10^{-4}	2.49×10^{-3}
	25	5.22×10^{-4}	3.87×10^{-3}
	53	3.68×10^{-4}	5.27×10^{-3}

Trends shown in this section can appear for the competition between Mg or Ca and other divalent trace metal cations. However, since Mn shows the smallest binding affinity to Chelex among divalent cations, competition effects with other divalent cations involving deviations from perfect sink will require Mg or Ca concentrations above the values typical of freshwaters. No competition effects are expected between trace metals themselves given their low concentrations and the large amount of Chelex used per disc.

When other less selective binding agents are used, competition effects are expected to be more noticeable. This applies to those used for both cations (e.g. a general cation exchange resin or a metal oxide) and anions (e.g. metal oxides).

4. Conclusions

Even though DGT was designed to obtain linear accumulations with time, for long deployments the uptake may be curved downwards for some cations due to equilibrium or competition effects. While linear accumulations indicate the plausibility of steady-state conditions, bending unequivocally indicates a decrease in the rate of metal binding. These various situations have been analysed in this work, which provides a set of approximate analytical expressions to reproduce the DGT accumulations as well as to calculate the bulk concentration when there are: kinetic limitations in the binding to the resin, Eqn. (2); saturation/equilibrium phenomena, Eqn. (5); or competition effects, Eqn. (9). The binding of Mg or Mn have been used to exemplify the use of these expressions. For the studied conditions, accumulations of Mg or Mn in single metal systems have provided examples of equilibrium effects. In a mixed system, the binding of Mg reduces the accumulation rate of Mn. Concentrations obtained with the simple approximate expressions reported in this work significantly improve the estimations based on perfect sink conditions.

Reference List

1. W. Davison, H. Zhang, In-situ speciation measurements of trace components in natural-waters using thin-film gels, Nature, 367 (1994) 546-548.

2. O. A. Garmo, O. Royset, E. Steinnes, T. P. Flaten, Performance study of diffusive gradients in thin films for 55 elements, Anal. Chem., 75 (2003) 3573-3580.

3. W. Davison, H. Zhang, Progress in understanding the use of diffusive gradients in thin films (DGT) – back to basics, Environ. Chem., 9 (2012) 1-13.

4. K. W. Warnken, H. Zhang, W. Davison, Accuracy of the diffusive gradients in thin-films technique: Diffusive boundary layer and effective sampling area considerations, Anal. Chem., 78 (2006) 3780-3787.

5. H. Zhang, W. Davison, Performance characteristics of diffusion gradients in thin films for the insitu measurement of trace metals in aqueous solution., Anal. Chem., 67 (1995) 3391-3400.

6. J. G. Panther, P. R. Teasdale, W. W. Bennett, D. T. Welsh, H. J. Zhao, Titanium Dioxide-Based DGT Technique for In Situ Measurement of Dissolved Reactive Phosphorus in Fresh and Marine Waters, Environ. Sci. Technol., 44 (2010) 9419-9424.

7. Y. L. Zhang, S. Mason, A. McNeill, M. J. McLaughlin, Optimization of the diffusive gradients in thin films (DGT) method for simultaneous assay of potassium and plant-available phosphorus in soils, Talanta, 113 (2013) 123-129.

8. J. G. Panther, R. R. Stewart, P. R. Teasdale, W. W. Bennett, D. T. Welsh, H. J. Zhao, Titanium dioxide-based DGT for measuring dissolved As(V), V(V), Sb(V), Mo(VI) and W(VI) in water, Talanta, 105 (2013) 80-86.

9. C. E. Chen, H. Zhang, G. G. Ying, K. C. Jones, Evidence and Recommendations to Support the Use of a Novel Passive Water Sampler to Quantify Antibiotics in Wastewaters, Environ. Sci. Technol., 47 (2013) 13587-13593.

10. H. P. van Leeuwen, Steady-state DGT fluxes of nanoparticulate metal complexes, Environ. Chem., 8 (2011) 525-528.

11. E. Navarro, F. Piccapietra, B. Wagner, F. Marconi, R. Kaegi, N. Odzak, L. Sigg, R. Behra, Toxicity of Silver Nanoparticles to Chlamydomonas reinhardtii, Environ. Sci. Technol., 42 (2008) 8959-8964.

12. R. Tantra, H. Bouwmeester, E. Bolea, C. Rey-Castro, C. A. David, J. M. Dogne, J. Jarman, F. Laborda, J. Laloy, K. N. Robinson, A. K. Undas, M. van der Zande, Assessing Suitability of Analytical Methods to Measure Solubility for the Purpose of Nano-Regulation, Nanotoxicology, 10 (2016) 173-184.

13. W. W. Bennett, P. R. Teasdale, D. T. Welsh, J. G. Panther, R. R. Stewart, H. L. Price, D. F. Jolley, Inorganic arsenic and iron(II) distributions in sediment porewaters investigated by a combined DGT-colourimetric DET technique, Environ. Chem., 9 (2012) 31-40.

14. W. W. Bennett, P. R. Teasdale, J. G. Panther, D. T. Welsh, D. F. Jolley, New Diffusive Gradients in a Thin Film Technique for Measuring Inorganic Arsenic and Selenium(IV) Using a Titanium Dioxide Based Adsorbent, Anal. Chem., 82 (2010) 7401-7407.

15. S. Mason, R. Hamon, A. Nolan, H. Zhang, W. Davison, Performance of a mixed binding layer for measuring anions and cations in a single assay using the diffusive gradients in thin films technique, Anal. Chem., 77 (2005) 6339-6346.

16. J. Santner, M. Larsen, A. Kreuzeder, R. N. Glud, Two decades of chemical imaging of solutes in sediments and soils - a review, Anal. Chim. Acta, 878 (2015) 9-42.

17. P. N. Williams, J. Santner, M. Larsen, N. J. Lehto, E. Oburger, W. Wenzel, R. N. Glud, W. Davison, H. Zhang, Localized Flux Maxima of Arsenic, Lead, and Iron around Root Apices in Flooded Lowland Rice, Environ. Sci. Technol., 48 (2014) 8498-8506.

18. Y. Pan, D. X. Guan, D. Zhao, J. Luo, H. Zhang, W. Davison, L. Q. Ma, Novel Speciation Method Based on Diffusive Gradients in Thin-Films for in Situ Measurement of Cr-VI in Aquatic Systems, Environ. Sci. Technol., 49 (2015) 14267-14273.

19. H. Stahl, K. W. Warnken, L. Sochaczewski, R. N. Glud, W. Davison, H. Zhang, A combined sensor for simultaneous high resolution 2-D imaging of oxygen and trace metals fluxes, Limnology and Oceanography-Methods, 10 (2012) 389-401.

20. F. Degryse, E. Smolders, I. Oliver, H. Zhang, Relating soil solution Zn concentration to diffusive gradients in thin films measurements in contaminated soils, Environ. Sci. Technol., 37 (2003) 3958-3965.

21. S. Mason, R. Harnon, H. Zhang, J. Anderson, Investigating chemical constraints to the measurement of phosphorus in soils using diffusive gradients in thin films (DGT) and resin methods, Talanta, 74 (2008) 779-787.

22. S. Tankere-Muller, H. Zhang, W. Davison, N. Finke, O. Larsen, H. Stahl, R. N. Glud, Fine scale remobilisation of Fe, Mn, Co, Ni, Cu and Cd in contaminated marine sediment, Mar. Chem., 106 (2007) 192-207.

23. L. Y. Chang, W. Davison, H. Zhang, M. Kelly, Performance characteristics for the measurement of Cs and Sr by diffusive gradients in thin films (DGT), Anal. Chim. Acta, 368 (1998) 243-253.

24. R. Dahlqvist, H. Zhang, J. Ingri, W. Davison, Performance of the diffusive gradients in thin films technique for measuring Ca and Mg in freshwater, Analytica Chimica Acta, 460 (2002) 247-256.

25. S. Tankere-Muller, W. Davison, H. Zhang, Effect of competitive cation binding on the measurement of Mn in marine waters and sediments by diffusive gradients in thin films, Analytica Chimica Acta, 716 (2012) 138-144.

26. J. G. Panther, P. R. Teasdale, W. W. Bennett, D. T. Welsh, H. J. Zhao, Titanium Dioxide-Based DGT Technique for In Situ Measurement of Dissolved Reactive Phosphorus in Fresh and Marine Waters, Environmental Science & Technology, 44 (2010) 9419-9424.

27. J. G. Panther, W. W. Bennett, D. T. Welsh, P. R. Teasdale, Simultaneous Measurement of Trace Metal and Oxyanion Concentrations in Water using Diffusive Gradients in Thin Films with a Chelex-Metsorb Mixed Binding Layer, Anal. Chem., 86 (2014) 427-434.

28. S. Mason, R. Hamon, A. Nolan, H. Zhang, W. Davison, Performance of a mixed binding layer for measuring anions and cations in a single assay using the diffusive gradients in thin films technique, Analytical Chemistry, 77 (2005) 6339-6346.

29. M. Jimenez-Piedrahita, A. Altier, J. Cecilia, C. Rey-Castro, J. Galceran, J. Puy, Influence of the settling of the resin beads on Diffusion Gradients in Thin films measurements, Anal. Chim. Acta, 885 (2015) 148-155.

30. J. Puy, R. Uribe, S. Mongin, J. Galceran, J. Cecilia, J. Levy, H. Zhang, W. Davison, Lability Criteria in Diffusive Gradients in Thin Films, J. Phys. Chem. A, 116 (2012) 6564-6573.

31. S. Mongin, R. Uribe, C. Rey-Castro, J. Cecilia, J. Galceran, J. Puy, Limits of the Linear Accumulation Regime of DGT Sensors, Environ. Sci. Technol., 47 (2013) 10438-10445.

32. J. Galceran, J. Puy, Interpretation of diffusion gradients in thin films (DGT) measurements: a systematic approach, Environ. Chem., 12 (2015) 112-122.

33. J. Puy, J. Galceran, C. Rey-Castro, in W.Davison (Ed.), Diffusive Gradients in Thin-Films for Environmental Measurements, Cambridge University Press, Cambridge, 2016, Ch.5.

34. J. L. Levy, H. Zhang, W. Davison, J. Puy, J. Galceran, Assessment of trace metal binding kinetics in the resin phase of diffusive gradients in thin films, Anal. Chim. Acta, 717 (2012) 143-150.

35. M. Eigen, R. Wilkins, The Kinetics and Mechanism of Formation of Metal Complexes, 49 ed., American Chemical Society, Washington, 1965.

36. J. L. Levy, H. Zhang, W. Davison, J. Puy, J. Galceran, Assessment of trace metal binding kinetics in the resin phase of diffusive gradients in thin films, Anal. Chim. Acta, 717 (2012) 143-150.

37. W. J. G. M. Peijnenburg, P. R. Teasdale, D. Reible, J. Mondon, W. W. Bennett, P. G. C. Campbell, Passive sampling methods for contaminated sediments: State of the science for metals, Integrated Environmental Assessment and Management, 10 (2014) 179-196.

38. W. W. Bennett, Maja Arsic., J. G. Panther, D. T. Welsh, P. R. Teasdale, in W.Davison (Ed.), Diffusive Gradients in Thin-films for environmental measurements, Cambridge University Press, Cambridge, 2016, Ch.4.

39. A. Altier, M. Jimenez-Piedrahita, C. Rey-Castro, J. Cecilia, J. Galceran, J. Puy, Accumulation of Mg to Diffusive Gradients in Thin Films (DGT) Devices: Kinetic and Thermodynamic Effects of the Ionic Strength, Anal. Chem., 88 (2016) 10245-10251.

40. Chelex 100 and Chelex 20 Chelating Ion Exchange Resin Instruction Manual; Bio-Rad Laboratories, 2013.